45. M.Hansen and K.Anderko, "Constitution of Binary Alloys", McGraw-Hill, New York, 1958.
46. L.A.Carapella, Metal Progress, 48, 297 (1945).
47. V.G.Kuznetsov, Izv.Sektora Fiz.-Khim.Anal., Inst.Obshch. Neorg.Khim.Akad.Nauk SSSR, 16, 68 (1948).
48. I.I.Kornilov, Izv.Akad.Nauk SSSR, Otd.Khim.Nauk, 475 (1950).
49. I.I.Kornilov, Izv.Akad.Nauk SSSR, Otd.Khim.Nauk, 980 (1953).
50. I.I.Kornilov, Izv.Akad.Nauk SSSR, Otd.Khim.Nauk, 392 (1954).
51. E.M.Savitskii and V.V.Kopetskii, Izv.Akad.Nauk SSSR, Otd. Tekh.Nauk, Seriya Metallurgiya i Toplivo, 157 (1962).
52. I.I.Kornilov and R.S.Polyakova, Izv.Akad.Nauk SSSR, Otd. Khim.Nauk, 565 (1962).
53. I.I.Kornilov and N.M.Matveeva, Uspekhi Khim., 31, 1076 (1962) [Russ.Chem.Rev., 512 (1962)].
54. I.I.Kornilov, Zhur.Neorg.Khim., 3, 571 (1958).
55. I.I.Kornilov, Dokl.Akad.Nauk SSSR, 128, 722 (1959).
56. N.S.Kurnakov, S.F.Zhemchuzhnyi, and M.I.Zasedatelev, Zhur.Russ.Fiz.-Khim.Obshch., 47, 871 (1915).
57. F.Weibke, Z.Elektrochem., 44, 209, 263 (1938).
58. P.I.Kripyakevich and E.E.Cherkashin, Izv.Sektora Fiz.--Khim.Anal., Inst.Obshch.Neorg.Khim.Akad.Nauk SSSR, 24, 59 (1954).
59. I.I.Kornilov and B.K.Vul'f, Uspekhi Khim., 28, 1087 (1959).
60. G.B.Bokii, B.K.Vul'f, and N.L.Smirnova, Zhur.Strukt. Khim., 2, 74 (1961).
61. G.V.Samsonov, Poroshkovaya Metallurgiya Akad.Nauk Ukrain.SSR, 2 (2), 3 (1962).
62. N.V.Grum-Grzhimailo, I.I.Kornilov, E.N.Pylaeva, and M.A.Volkova, Dokl.Akad.Nauk SSSR, 137, 599 (1961).
63. I.I.Kornilov and V.V.Glazova, Dokl.Akad.Nauk SSSR, 130, 33 (1963).
64. O.Kubaschewski and E.Ll.Evans, "Metallurgical Thermochemistry" (Translated into Russian), Inostr.Lit., Moscow, 1954.
65. Yu.M.Golutvin, "Teploty Obrazovaniya i Tipy Khimicheskoi Svyazi v Neorganicheskikh Kristallakh" (Heats of Formation and Chemical Bond Types in Inorganic Crystals), Izd.Akad. Nauk SSSR, 1962.
66. N.V.Ageev, Zhur.Neorg.Khim., 3, 537 (1958).
67. I.I.Kornilov and N.M.Matveeva, Dokl.Akad.Nauk SSSR, 139, 4 (1961).
68. S.T.Konobeevskii, Izv.Sektora Fiz.-Khim.Anal., Inst. Obshch.Neorg.Khim.Akad.Nauk SSSR, 16, 19 (1943).
69. G.V.Samsonov, L.Ya.Markovskii, A.F.Zhigach, and M.G.Valyashko, "Bor, Ego Soedineniya i Splavy" (Boron, Its Compounds and Alloys), Izd.Akad.Nauk Ukrain.SSR, Kiev, 1960.
70. G.V.Samsonov and Ya.S.Umanskii, "Tverdye Soedineniya Tugoplavkikh Metallov" (Hard Compounds of High-Melting Metals), Metallurgizdat, 1957.
71. G.V.Samsonov, "Silitsidy i Ikh Ispolzovanie v Tekhnike" (Silicides and Their Industrial Applications), Izd.Akad.Nauk Ukrain.SSR, 1959.
72. G.V.Samsonov and L.L.Vereikina, "Fosfidy" (Phosphides), Izd.Akad.Nauk Ukrain.SSR, 1961.
73. G.V.Samsonov and S.V.Rodzinskaya, Uspekhi Khim., 30, 60 (1961) [Russ.Chem.Rev., 28 (1961)].
74. I.I.Kornilov, "Sbornik Dokladov na Soveshchanii po Teorii Metallicheskikh Splavov" (Papers Presented to the Conference on the Theory of Alloys), Izd.Akad.Nauk SSSR, 1952.
75. W.E.Garner, "Chemistry of the Solid State", Butterworth, London, 1955; *ibid.* (Translated into Russian), Inostr.Lit., Moscow, 1961.
76. I.I.Kornilov, Izv.Sektora Fiz.-Khim.Anal., Inst.Obshch. Neorg.Khim.Akad.Nauk SSSR, 20, 294 (1950).
77. A.M.Rubinshtein, Uspekhi Khim., 21, 1287 (1952).
78. V.I.Arkharov, "Okislenie Metallov" (Oxidation of Metals), Metallurgizdat, 1945.
79. O.Kubaschewski and B.E.Hopkins, "The Oxidation of Metals and Alloys" (Translated into Russian), Metallurgizdat, 1961.
80. D.V.Ignatov and R.D.Shamgunova, "O Mekhanizme Okisleniya Splavov na Osnove Nikela" (Mechanism of the Oxidation of Nickel-Base Alloys), Izd.Akad.Nauk SSSR, 1960.
81. M.Yu.Bal'shin, "Poroshkovaya Metallurgiya" (Powder Metallurgy), Mashgiz, 1948.
82. F.Eisenkolb, "Die neuere Entwicklung der Pulver-metallurgie", Verlag Technik, Berlin, 1955.
83. I.I.Kornilov, Dokl.Akad.Nauk SSSR, 81, 597 (1951).

Baikov Institute of Metallurgy

U. D. C. 546.26-162

PYROGRAPHITE (PREPARATION, STRUCTURE, PROPERTIES)

A. S. Fialkov, A. L Baver, N. M. Sidorov, M. L Chaikun, and S. M. Rabinovich

CONTENTS

I. Introduction 46
II. Short description of the methods for the preparation of pyrographite 47
III. Physicochemical processes occurring during the preparation of pyrographite 47
IV. Structure of pyrographite 50
V. Properties of pyrographite 52
1. Density 52
2. Hardness 53
3. Linear thermal expansion 53
4. Mechanical properties 53
5. Thermal conductivity 54
6. Electrophysical properties 54
VI. Uses of pyrographite 56

I. INTRODUCTION

Pyrolytic graphite is the product of the pyrolysis of hydrocarbons on surfaces heated to 1000–2500°C. In recent years this material has attracted very considerable attention from research scientists, technologists, and engineers working in various fields of science and technology. This is because of the many quite unique properties of pyrolytic graphite. Its strength at temperatures

above 2500° exceeds that of any other known material. It has the highest ratio of strength to density (Fig. 1); its thermal and electrical properties show a very characteristic and highly developed anisotropy, the thermal conductivity being very low in the direction normal to the plane of deposition.

The particular method of preparation used ensures that pyrolytic graphite is practically a non-porous material.

Pyrolytic graphite (or pyrographite) also has great practical interest as one of the starting elements used in the production of other pyrolytic materials (pyrometals, pyrocarbides, pyrocarbonitrocompounds, etc.). The results of investigations on the production, structure, and properties of pyrographite can evidently be used to a great extent in the characterisation of these other pyrolytic materials. This is particularly true of the various pyrocarbides and pyrocarbonitrides, which can be expected to play an increasing part in the immediate future.

The study of the effect of formation conditions upon the structure and properties of pyrographite is very interesting also from a purely scientific point of view. Single crystals of graphite large enough to permit measurements of its physical and chemical properties have not yet been prepared. The properties of graphite are commonly studied using polycrystalline two-component or multicomponent materials, prepared by a kind of ceramic technique from graphitised carbon particles and a binding medium. The properties of specimens of these materials depend on many extraneous factors, such as the degree of dispersion of the particles, complex contact phenomena, uncontrolled porosity, etc.

The properties of pyrographite, which is prepared without the use of a binder, depend only on purely structural arrangements. Therefore, pyrographite is very attractive as a subject for investigation, especially in studies of the electrophysical properties of graphitised carbons.

II. SHORT DESCRIPTION OF THE METHODS FOR THE PREPARATION OF PYROGRAPHITE

Pyrolytic carbon can be prepared by two paths:

1. Carbonisation, i.e. pyrolytic decomposition of carbon-containing materials in a condensed phase.

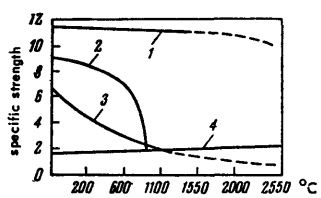


Fig. 1. Effect of temperature on the specific strength (ratio of strength to specific gravity) of pyrographite and of some other materials:
1) pyrographite, along the *a* axis;
2) stainless steel;
3) tungsten;
4) graphite.
[The units of specific strength are not given; it is often given as strength/density (Ed. of Translation).]

2. Deposition of carbon, i.e. homogeneous or heterogeneous decomposition of hydrocarbon gases and vapours.

In addition, pyrographites can be classified according to their preparation temperature into low-temperature (produced at 800–1100°) and high-temperature materials (produced at temperatures above 2000°). Low-temperature pyrographite can be prepared by deposition and by carbonisation methods, whereas the high-temperature form is usually prepared exclusively by deposition.

In the deposition method[1,2], hydrocarbons are made to impinge on a heated surface either in a stream of carrier gas at atmospheric pressure or by diffusion of gaseous hydrocarbons or the vapours of liquid hydrocarbons in an evacuated reactor. The carrier is usually an inert gas (nitrogen, argon, or helium).

There are many reports[3-14] of the use of various amounts of hydrogen in the reaction mixture, added to decrease the rate of pyrolysis.

The solid deposition substrate, usually made of graphitised carbon, is heated either by induction or by a direct or an indirect resistance heater. Maintaining a constant temperature during the deposition seems to be very important. Many vacuum processes for making pyrographite have been described[6-8,15]. They differ mainly in the degree of vacuum used (from 10^{-1} mmHg[6-8] to 10^{-7} mmHg[15]).

III. PHYSICOCHEMICAL PROCESSES OCCURRING DURING THE PREPARATION OF PYROGRAPHITE

The extreme thermal decomposition of hydrocarbons has been investigated by many workers[1,2,7,8,11-61]. One of the earliest papers on the mechanism of the thermal decomposition of hydrocarbons was published by Berthelot[41] as long ago as in 1866.

There are a number of opinions regarding the mechanism of the high-temperature pyrolysis of hydrocarbons.

According to Tesner and his coworkers[20,22-35], and also some non-Soviet authors[12-14,21], the decomposition of hydrocarbons on surfaces heated to high temperatures involves the direct dissociation of hydrocarbon molecules into carbon and hydrogen. However, Wheeler considers[13] that the decomposition proceeds through the adsorption of a hydrocarbon molecule on the surface, followed by dehydrogenation of the adsorbed molecule.

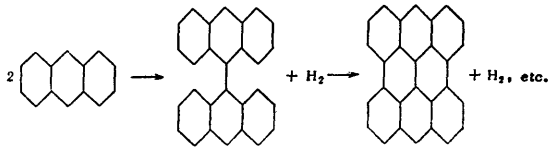
At low concentrations, the formation of pyrolytic graphite can only occur heterogeneously, since gaseous reactions are precluded. According to Tesner and Rafal'kes[25,29], the rate of formation of a pyrolytic film at 800–1000° is directly proportional to the hydrocarbon concentration, i.e. the reaction is of the first order with respect to the hydrocarbon. As the concentration is raised, the probability of gaseous reactions increases, and at a well-defined critical concentration (which Tesner calls[29] the "threshold" concentration) the reactions in the gas phase begin to produce carbon in a very fine state of subdivision (soot). However, the formation of carbon at the heated surface continues even when soot begins to precipitate in the reaction volume.

Tesner and his coworkers believe[20,22-26,29] that the inhibition by hydrogen of the pyrolysis reaction results from activated adsorption of hydrogen on the surface or from Stefan flow of hydrogen from the surface[31]. According to other workers[12-14,21], the effect of hydrogen can be

explained by a shift of the equilibrium towards the reactants.

An alternative mechanism suggested for the formation of pyrocarbon states that hydrocarbons are dehydrogenated during pyrolysis to give complex polymeric aromatic compounds, which are ultimately converted into solid particles. According to this hypothesis, pyrocarbon is an aggregate of extremely high-melting polymeric hydrocarbons[1,8,9,17,38,39,51]. This provides a fairly simple description of the pyrolysis of aromatic compounds. Kinney *et al.*[1,38,39] studied the pyrolysis of benzene and some of its derivatives and found that the yield of pyrocarbon increases with the molecular weight of the aromatic compound, and that under these conditions fission of the aromatic rings does not occur, since low-molecular-weight acetylene hydrocarbons are not detected in the effluent gases even when hydrogen is used as the carrier gas — hydrogen should favour the formation of these compounds. Gases which usually accompany acetylene (e.g. ethylene) are also absent[1].

These features of the pyrolysis of aromatic compounds were confirmed by the work of Rudenko[2], who demonstrated the absence of products from the decomposition of the benzene ring in the gases obtained from the pyrolysis of benzene. In a study of the pyrolysis of anthracene, Kinney *et al.*[39] obtained resinous products as well as solid carbon. Chromatographic analysis of the resin revealed the presence of the anthracene condensation products 9,10-diphenylanthracene and 1,2,5,6-dibenzanthracene. A fraction having an ultraviolet adsorption spectrum identical to that of 9,9′-bianthryl was isolated. Multiple dehydrocondensation, analogous to the process observed during coking of petroleum products[52], obviously occurs:



The presence of diphenylanthracene is due to the excess hydrogen, which causes partial rupture of the aromatic rings. The reaction occurs on the surface as a result of sorption and dehydrogenation of the hydrocarbons, with formation of highly condensed products unlikely to diffuse into the gas phase. On this model, hydrogen lowers the yield of carbon by causing hydrogenation.

The fact that hydrogen has a more pronounced effect in the pyrolysis of non-aromatic hydrocarbons[22] lends support to these views, since these compounds evolve more hydrogen.

Grisdale and coworkers[17,50] have suggested a similar mechanism, but they believe that condensation of aromatic rings occurs in the gas phase, with subsequent deposition of high polymers on the surface. The main evidence in favour of their mechanism is the frequent appearance of spherical drop-like formations on the pyrographite surface. However, the authors do not advance any really serious arguments in support of their views. The attempt by Conroy *et al.*[38] to detect highly condensed aromatic hydrocarbons in the gas phase was unsuccessful.

Other workers[15,40-49,51,53,58,60] point out that the pyrolysis of hydrocarbons involves a free-radical mechanism. Thus, the pyrolysis is characterised by the so-called "wall effect", i.e. the recombination of radicals at the walls of the reaction chamber or at other surfaces within the reaction zone.

In addition to wall recombinations (chain breaking), reactions between radicals occur also in the reaction volume: these lead to a whole spectrum of more complex hydrocarbons.

Hague and Wheeler[44] consider that the initial act in the decomposition of methane is the formation of hydrogen and a methyl radical.

Bone and Coward[11], and also Fischer[36,45], are of the opinion that the first stage in the decomposition of methane involves the formation of the radicals CH_3, CH_2, and CH.

Rice *et al.*[46] have shown that gaseous hydrocarbons, in particular butane and propane, when passed through a quartz tube heated to 800–1000° at a pressure of 10 mmHg, can destroy Pb, Zn, and Sn mirrors at a distance of 30–40 mm from the reaction zone. This is evidence for the presence of free radicals.

Rice and Dooley[47] showed that the main reaction occurring during the pyrolysis of ethane is dissociation into free radicals rather than splitting off of molecular hydrogen, as had been assumed by many other workers.

Poltorak and Voevodskii[58] used deuteration to prove that the pyrolysis of propane occurs by a radical mechanism; this relies on the ready exchange between deuterium and the hydrogen of free radicals. Propane was pyrolysed in the presence of deuterium, and deuterium was detected in the hydrocarbons produced by the reaction in amounts which were not a function of reaction time.

Shantarovich and Pavlov[60] studied the kinetics of the thermal cracking of methane on porcelain and carbon black surfaces. The shape of the kinetic curves given by the cracking reaction on carbon black is indicative of autocatalysis, the acceleration being due to the development of a chain process. The authors conclude that the decomposition of methane occurs by the following scheme:

$$CH_4 \rightarrow CH_3 + H,$$
$$H + CH_4 \rightarrow CH_3 + H_2,$$
$$CH_3 \rightarrow CH_2 + H,$$
$$CH_3 + CH_4 \rightarrow C_2H_6 \text{ or } CH_2 + CH_4 \rightarrow 2CH_3.$$

Retardation by hydrogen is probably associated with chain breaking by hydrogen, and with displacement of the equilibrium towards the reactants. A critical inspection of the suggested mechanisms prompts the following remarks.

The direct decomposition mechanism lacks adequate experimental proof. The authors quote only activation energy values, which are found to be of the same order as the energy of the C–H bond. The formation of carbon from aromatic hydrocarbons is inexplicable on the basis of this mechanism.

The multiple dehydrogenation mechanism is more realistic, and can claim sounder experimental confirmation. The retarding effect of hydrogen on the rate of formation of pyrolytic graphite is an additional indirect proof of the dehydrogenation scheme for the formation of carbon films. However, in view of the work of Stehling and others[40,42], a purely condensation type of mechanism is unacceptable. It is clear that this mechanism occurs in conjunction with radical polymerisation.

The radical mechanism for the formation of pyrolytic graphite appears to us to be the most probable, since it has quite unambiguous experimental confirmation. We may therefore describe the formation of pyrolytic graphite as follows.

When the hydrocarbon molecules enter the high-temperature region, they are split into free radicals. With aromatic hydrocarbons, fissure occurs at C–H bonds, whereas with aliphatic hydrocarbons the C–C bond is mainly affected[61]. The hydrogen atoms produced by the cleavage of the molecules react with the incandescent carbon surface to give lower hydrocarbons and their radicals: CH_4, $CH_3^{\cdot}$, $C_2H_5^{\cdot}$, C_2H_6, C_2H_2, $C_2H^{\cdot}$, and $^{\cdot}C\equiv C^{\cdot}$. These produce active centres on the carbon surface, able to react with newly formed radicals. Extensive dehydrogenation and consolidation of the radicals occurs before these can enter into the reaction from the gas phase.

Thus, a large number of local interactions occurs simultaneously at many sites. The resulting film of pyrolytic graphite is a true replica of the outline of the substrate surface, showing that the carbon atoms cannot move over the surface at high temperatures.

The hydrocarbon residues, being on a hot surface whose energy is higher than that of the surrounding gas phase, can split off hydrogen and react with neighbouring residues, thus forming a crystal lattice.

Since aromatic structures are thermodynamically the most stable at high temperatures, cyclisation takes place on the surface, with formation of a graphitic network. The distance between graphitic planes, and the development of three-dimensional order, depend on the deposition temperature. At low hydrocarbon concentrations (whether under atmospheric pressure or in a vacuum) and at temperatures of the order of 2000° the fundamental processes take place on the surface. At temperatures above 2800° in a vacuum the vapour pressure above the carbon surface is so high[62] that the radicals cannot reach the surface, and decomposition of the hydrocarbons occurs in the gas phase.

At relatively low temperatures (~ 1100°) the energy of the surface is much lower, and the radicals can penetrate inside the pores of the carbonaceous material and decompose there. This is the basis of the bulk densification of graphitised carbon articles, designed to impart greater strength and hardness and lower permeability to gases[19,20]. The process should be carried out at low concentrations, for otherwise the orifices of the pores may become rapidly covered over, and prevent the penetration of the hydrocarbon into the material.

Simultaneously with the surface decomposition, reactions leading to the formation of biphenyl, acetylene, hydrogen, etc. take place in the bulk[43]. The rate of these reactions is determined by the concentration of the vapours undergoing pyrolysis and also by the temperatures and duration of the process and by the physicochemical properties of the surface.

The influence of temperature and of partial pressure of the gas on the rate of growth of the carbon film was investigated by Murphy *et al.*[54], who used the logarithmic equation of Chen *et al.*[63] to describe the effect of these factors:

$$\log\left(\frac{m}{pT}\right)=\log\left[\frac{\pi D}{\rho L}\delta K\frac{k}{h}\left(\exp\frac{\Delta S^*}{R}\right)\right]-0.4343\,\frac{\Delta H^*}{RT},$$

where m is the rate at which the electrical conductance increases, p the partial pressure of the hydrocarbon, D the diameter of the film of pyrographite, ρ the electrical resistivity of the film, L the length of the film of pyrographite, δ the thickness of a monatomic layer of carbon in the film of pyrographite, K the rate constant for the growth of a monatomic layer, k Boltzmann's constant, h Planck's constant, ΔS^* the entropy of activation under standard conditions, ΔH^* the activation energy standard conditions, R the gas constant, and T the absolute temperature.

The rate constants measured experimentally for the pyrolysis of benzene, toluene, and methane are plotted against $1/T$ in Fig. 2. The linear plot shows that the reaction rate is quite low at temperatures below 860°, but becomes very large above 940°.

Similar kinetic curves were reported by Mar'yasin and Tesner[23,24], who studied the kinetics of the deposition of pyrographite films by the pyrolysis of methane in the temperature range 1400–1700°. This indicates that the temperature coefficient of the pyrolysis reaction rate is high. Between 1600° and 1800° this coefficient can apparently exceed the temperature coefficient which determines the lowering of the activation energy attending the ordering of the structure of the pyrographite film. This results in the phenomenon of structure disordering described below, and causes a decrease in the density of pyrographite in this temperature range.

The influence of the surface on the production of pyrolytic graphite needs special consideration.

Kobozev[56], in his study of the cracking of methane to acetylene, investigated the possible catalytic effect of the surface in the pyrolysis of methane to carbon. He found that the yield of carbon on the walls of the reactor was increased 50- to 100-fold when quartz or porcelain vessels were used. The reaction was typically catalytic, as shown also by the very specific action of various materials, depending on the type of surface, which was observed during a search for catalytic poisons to suppress the pyrolysis of methane to carbon.

Benevolenskaya and Kel'tsev[59] state that active alumina surfaces produce the most extensive decomposition of hydrocarbons undergoing cracking. At 1300° the hydrogen content of the effluent gases was as high as 96–97%.

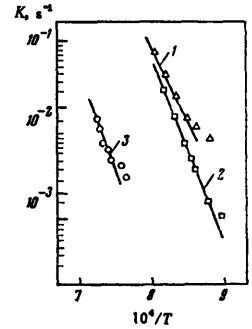


Fig. 2. Temperature variation (after Murphy *et al.*[54]) of the rate constant (K) for the pyrolysis of: 1: 1) toluene; 2) benzene; 3) methane.

Kinney and Del Bel[1] studied the pyrolysis of aromatic hydrocarbons from benzene to chrysene on different surfaces. They found, in particular, that the rate of pyrolysis (e.g. of anthracene to carbon) increases with the amount of coke present in the reactor, which suggests a heterogeneous catalytic reaction. The rate of reaction is increased also by silicon, mullite, and quartz, the quartz being by far the least effective.

According to Holdeman and Botty[55], heavy metals are the most active catalysts for the formation of pyrolytic carbon. They believe that the cracking of methane to carbon at temperatures up to 1000–1200° is a purely surface catalytic process. The actual catalyst in this case is either adsorbed carbon or the substrate surface, modified by the reducing action of hydrocarbon radicals and hydrogen at these temperatures.



Fig.3. Electron diffraction pattern of pyrographite.

IV. STRUCTURE OF PYROGRAPHITE

The remarkable properties of pyrographite are very much bound up with the structure of the material. This is particularly true of its highly developed anisotropy.

We know[64] that the various kinds of graphitic carbon material have in common a highly polymeric arrangement of the carbon atoms, which exist in hexagonal planes of different sizes and differently oriented in space.

In the most highly ordered state (graphite single crystals) the hexagonal planes of carbon atoms are stacked in the sequence ABAB. The interatomic distance in the six-membered rings is 1.42 Å, and between the symmetrically disposed planes it is 6.71 Å. In the hexagonal graphite lattice, three σ electrons form strong covalent bonds with three neighbouring atoms in the plane, and the fourth electron forms a weak π bond with a carbon atom from a neighbouring plane. The highly anisotropic properties in two mutually perpendicular directions is a direct consequence of this arrangement.

The opposite limiting case, a completely disordered state, corresponds to a statistically indeterminate distribution of the separate carbon planes over the volume of the material, the binding between the planes involving hetero-atoms, functional groups, or linearly polymerised carbon atoms.

However, this is an extreme case. In practice, even the most disordered carbonaceous materials consist of stacks of hexagonal planes which are mutually parallel, oriented with respect to the normal, and have dimensions of the order of 25 Å in thickness and 35 Å in diameter. These crystallites are bound together by the uncompensated valencies of the corner atoms, and also by the linearly polymerised carbon, hetero-atoms, etc. already mentioned.

Between these two extremes we find a whole range of intermediate structures[65]. Their distinguishing feature is the fact that the size of the crystallites in the direction of *a* axis varies from 50 to a few hundred Ångstrom units, and that only two-dimensional order persists. This means that orientation is complete only with respect to the normal to the crystallites.

Pyrographite is typical of the class of polycrystalline intermediate structures. However, it is distinguished by a high degree of preferential crystal orientation, observed in the aggregates of crystallites. The evidence for this is the electron diffraction pattern shown in Fig. 3 and the clearly developed hexagonal symmetry of the reflection patterns. X-Ray diffraction studies[66,67] have shown that the individual crystallites have a well-developed texture of (002) planes parallel to the deposition surface (Table 1).

This crystallographic picture is in good agreement with the results obtained by Fialkov *et al.*[68] in an X-ray structural investigation of natural graphites which had been made amorphous.

Other diffraction work has shown[8,67,69] that the degree of orientation of the hexagonal planes with respect to the deposition surface increases at higher deposition temperatures. The preferential orientation of pyrographite as a function of deposition temperature is assessed by X-ray diffraction[67] from the intensity of the (002) reflections obtained when the deposition surface is aligned at various angles to the incident beam. The degree of preferential orientation was evaluated[67] as the ratio of n_{max} to n_{min}, the relative intensities obtained with the deposition surface perpendicular and parallel to the incident X-ray beam.

Bragg and Packer[70], from measurements of the integral intensity of the (002) line, constructed a plot of this parameter (expressed in arbitrary units) against the inclination of the specimen (α) to the incident beam. They showed (Fig. 4) that the intensity of the (002) line varies linearly with α [Fig. 4 shows that the logarithm of the intensity varies linearly with α^2 (Ed. of Translation)] for specimens deposited at 1950° (*1*) and 2100° (*2*). Heating at 3000° for various times (curves *3* and *4*) introduced some departures

TABLE 1. X-Ray diffraction analysis of pyrographite.

Specimen	Interplanar spacing, d_{002}, Å	Crystallite size along *a* axis, L_a, Å	Degree of graphitisation (Ref. 71)
Prepared[66] in induction-heated vacuum furnace at 2300°	3.38	300	0.57
Prepared[66] in induction-heated vacuum furnace at 2400°	3.35	600	1.0
Prepared[66] in a vacuum resistance furnace at 2100°	3.42	235	0.07
Prepared[66] in a vacuum resistance furnace at 2500°	3.37	—	0.78

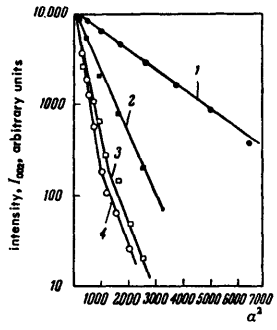


Fig. 4. Variation of the intensity I_{002} with the angle of incidence of the X-ray beam (after Bragg and Packer [70]) for different specimens of pyrographite, deposited: 1) at 1950°; 2) at 2100°; 3) at 2100°, followed by heat treatment for 5 min at 3000°; 4) treated for 25 min at 3000°.

TABLE 2. Influence of temperature and method of heating of the deposition surface upon the degree of preferential orientation.

Deposition temperature, °C	Method of heating	Subsequent heat treatment	Preferential orientation		Literature references
			n_{max}/n_{min}	$\chi_\perp/\chi_\parallel$	
1	2	3	4	5	6
2100	in resistance furnace (at atmospheric pressure)	none	—	8	10
2100	in resistance furnace (at atmospheric pressure)	none	—	11	10
2100	in resistance furnace (at atmospheric pressure)	heated to 2900°	—	16	10
2300	in resistance furnace (at atmospheric pressure)	heated to 2900°	—	17	10
2100	in resistance furnace (at atmospheric pressure)	heated to 3400°	—	24	10
2300	in resistance furnace (at atmospheric pressure)	heated to 3400°	—	40	10
1700	induction (*in vacuo*)	none	5	—	88
1700	induction (*in vacuo*)	3 h at 2500°	5	—	88
2400	induction (*in vacuo*)	none	2000	—	88
2100	in resistance furnace (*in vacuo*)	none	2000	—	88
2500	in resistance furnace (*in vacuo*)	none	4000	—	88

from linearity. However, Fig. 4 justifies the general conclusion that the (002) planes of the crystallites in pyrographite show a gaussian distribution, which can be expressed in the form:

$$I(\alpha) = I_0 \exp(\alpha^2/2\sigma^2),$$

where σ is the variance of the distribution.

At higher preparation temperatures, and after high-temperature treatment, σ decreases. Measurements of the diamagnetic susceptibility of a pyrographite film in the above-mentioned directions are a good method for evaluating structural anisotropy [10].

Data on the degree of preferential orientation as a function of deposition temperature and method of heating are reproduced in Table 2. It can be seen that the value of n_{max}/n_{min} varies from 5 at 1700° to approximately 4000 at 2500°.

The magnetic measurements reveal quite substantial changes in anisotropy after heat treatment (up to 3400°) of specimens prepared at 2100–2300°.

At temperatures of 2200–2300° and above, the pyrographite begins to develop three-dimensional order. This transition is preceded by a steady increase in crystallite size with temperature (both the height L_c and the diameter L_a), and by a decrease in interplanar spacing (Table 1). The transition manifests itself by the appearance and development of a (112) X-ray structural reflection, detected by the increase in the ratio of line intensities I_{112}/I_{110}.

Another quantitative test of the incipient three-dimensional ordering is provided by the sharp increase in electrical and thermal anisotropy. Taking a value of approximately 3.42 Å for the interlayer distance in the disordered state, and 3.355 Å in the single crystal, Kasatochkin and Kaverov [71] proposed the parameter γ for estimating the degree of graphitisation:

$$\gamma = \frac{3.425 - C_0/2}{3.425 - 3.355} = \frac{3.425 - C_0/2}{0.065},$$

where $C_0/2$ is the measured interlayer distance of the specimen.

Fig. 5 shows the variation of the three-dimensional ordering parameter of pyrographite with deposition temperature. By using induction heating (curve *1*), values varying between 0 and 1 can be obtained in the temperature range 1700–2400°.

These changes are characteristic of all types of graphitic carbon showing good graphitisation (homogeneous graphitisation, in Franklin's terminology [72]). When heating is by passage of an electric current through the specimen on which deposition is taking place (*cf.* curve *2* of Fig. 5), the graphitisation parameter is much lower. The difference between the two methods of heating is most probably due to an increasing thermal isolation of the pyrographite layer on the heater, causing a decrease in deposition temperature with increasing distance from the original surface of the heater.

Blackman and Ubbelohde [69] have published photometric curves obtained in an X-ray diffraction study of individual specimens of pyrographite of different thickness. Fig. 6 shows that the (*h*0*l*), (*hkl*), and (00*l*) lines decrease in intensity and increase in width as the thickness of the deposit increases, indicating a decrease in the degree of three-dimensional order with increasing separation from the original deposition surface.

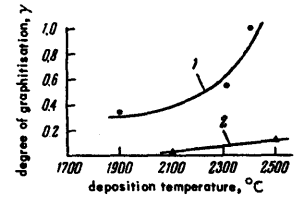


Fig. 5. Effect of deposition temperature and method of heating on the parameter for three-dimensional structural ordering in pyrographite:
1) heating in induction furnace;
2) heating in resistance furnace.

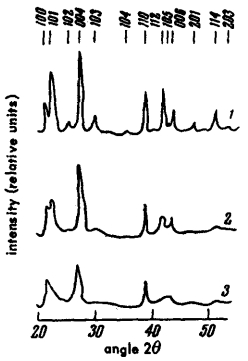


Fig. 6. Photometric traces from an X-ray diffraction study[69] of pyrographite, taken at various distances from the basal deposition plane:
1) 0.33 mm; 2) 0.49 mm; 3) 0.59 mm.

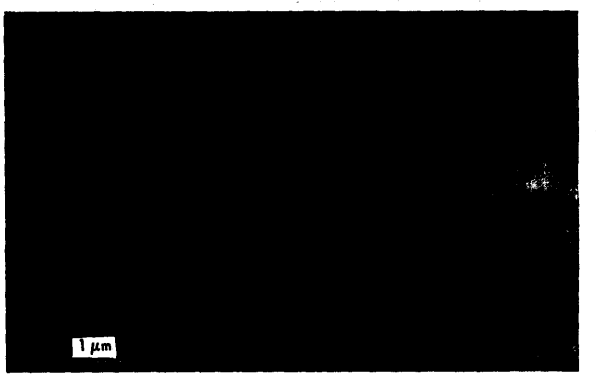


Fig. 8. Structure of pyrographite, observed in an electron microscope (× 8400).

Quite sharp differences in character between the resulting structures are revealed by the X-ray diffraction data for deposits of pyrographite obtained by Collingan and Galasso[37]. These authors showed that the structure of pyrographite is not a function of temperature only. Thus, they report that the (*hkl*) lines of specimens prepared at 1900° in an induction-heated furnace are sharper than those of specimens produced in a resistance furnace at 2200° and 2300°. It is right to point out, in this connection, that the deposition temperature is not a unique and sufficient criterion for the formation of the pyrographite structure. In addition to the temperature and to the method of heating, the composition and pressure of the gas phase, the gas flow rate, etc., can be expected to have a definite effect on the structure.

Fig. 7 shows a typical pyrographite microstructure, consisting of columnar formations of conical shape. As shown by X-ray diffraction, the hexagonal carbon planes are preferentially oriented normally to the conical formations, whose dimensions are typically a few microns. At higher deposition temperatures the columnar formations become dispersed[9,73,120].

High-temperature plastic deformation at 2750° tends to convert (10) lines into (100) and (101) lines. Thus, the degree of three-dimensional order — assessed by the increase in intensity of (101) lines — increases with the amount of plastic deformation[74]. Examination of pyrographite[75] in the electron microscope has revealed polygonal formations with a very fine internal structure.

The present authors have been able to detect[120] subgrains of less than 0.1 μm diameter in pyrographite preparations in the electron microscope (Fig. 8), thus confirming earlier reports[75,76].

V. PROPERTIES OF PYROGRAPHITE

1. Density

The specific gravity of polycrystalline graphitised carbon materials is one of their most important characteristics. This criterion is also very informative with pyrolytic graphite.

The variation of density with deposition temperature has been described by Brown and his coworkers[7,8,73,77].

On the curve of density against deposition temperature (Fig. 9) we may distinguish the following sections: (1) 1000–1400°; (2) 1400–1700°; (3) 1700–2000°; (4) 2000–2500°.

It can be assumed that the density of a pyrolytic graphite deposit is controlled by two main factors: (1) the mobility of carbon atoms on the deposition surface (the rate of

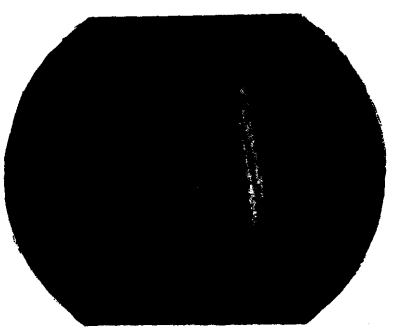


Fig. 7. Microstructure (× 50) of pyrographite, prepared by the authors[120] *in vacuo* at 2100° in a resistance furnace.

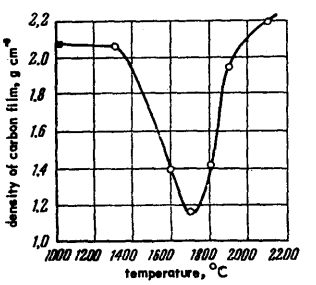


Fig. 9. Variation in density of pyrographite with temperature (after Brown and Watt[8]).

reorganisation of the crystallites); (2) the size of the hydrocarbon radical involved in the decomposition process at the surface.

In the temperature region 1000–1400° the mobility of carbon atoms is low and the hydrocarbon radicals are small, so that the resulting deposits are weakly oriented and have a high density (2.0–2.1 g cm^{-3}). Between 1400° and 1700° the activation energy of the dehydrogenation processes decreases, and the rate of formation of hexagonal carbon planes increases. At the same time, the hydrocarbon radicals become very much larger. The net result of these effects is to produce poorly oriented deposits of quite low density (as low as 1.29 g cm^{-3} at 1700°).

At temperatures above 1700°, there is a sharp increase in the mobility of the hexagonal carbon planes, and fairly well oriented deposits of high density are formed in spite of the possibility of larger hydrocarbon radicals (the density exceeds 2.22 g cm^{-3}, and approaches the value of 2.26 g cm^{-3} found in single crystals[9]).

The density and other properties of the deposits are not a function of the nature of the hydrocarbon[7,8,20,73,77].

Studies of gas permeability[19,73] have shown that open pores are absent. This suggests that the change in density of pyrographite is due exclusively to changes in the packing of the crystallites and of their constituent hexagonal layers.

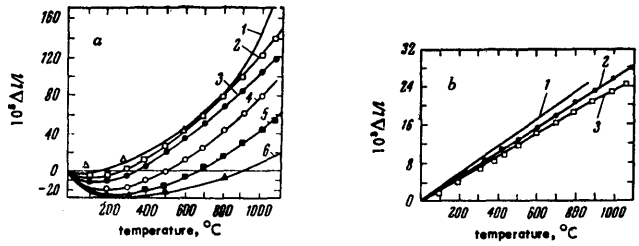


Fig.10. Temperature variation of linear thermal expansion for pyrographite and single crystals of natural graphite in two mutually perpendicular directions[80]:
a) along the *a* axis:
1) of specimens prepared at at atmospheric pressure;
2) of coarsely crystalline structures prepared *in vacuo* and heat treated for 3 h at 2700°;
3) of coarsely crystalline structures prepared *in vacuo*;
4) of microcrystalline structures prepared *in vacuo*;
5) of microcrystalline structures prepared *in vacuo* and heat treated for 3 h at 2700°;
6) of single crystals of natural graphite;
b) along the *c* axis:
1) of single crystals of natural graphite;
2) of pyrographite as prepared;
3) of pyrographite heat treated for 1 h at 3000°.

2. Hardness

The hardness of pyrographite is a function of the deposition temperature, and shows a maximum at 1000–1520° according to Tesner and Timofeeva[20]. This is because the material prepared at these temperatures has the maximal amount of structural disorder and the best developed system of cross-linking bonds.

The hardness of pyrographite has been found to be higher in the deposition direction than at right angle to it.

According to Lozier and Manofsky[9], pyrographite of density 2.2 g cm^{-3} (deposited at 2000°) is nine or ten times harder in the deposition direction than ordinary polycrystalline graphite. Subsequent heat treatment at 3000° produces a four- or five-fold decrease in hardness, both in the deposition direction and perpendicular to it.

3. Linear Thermal Expansion

Pappis found[78-81] that the linear thermal expansion coefficient of pyrographite is directly related to the crystallographic anisotropy of the material. Fig. 10 shows the changes in linear thermal expansion of pyrographite specimens in two mutually perpendicular directions as a function of the temperature and method of preparation, and of heat treatment. An increase in the deposition temperature, and high-temperature heat treatment, cause the linear expansion coefficient in both directions to approach the corresponding values for single crystal specimens[9]. However, as Fig. 10 shows, the two values differ very considerably. This is because the linear expansion coefficient of pyrographite is sensitive not only to crystallographic factors but also to the microstructure, and to the internal stresses which develop in the material. Heat treatment at 3000°, by favouring the growth of structural anisotropy, also relieves internal stresses in the material. Specimens prepared at atmospheric pressure (unlike those prepared in a vacuum) do not show a negative temperature coefficient between 0° and 700° in the direction parallel to the deposition surface. This indicates a considerable decrease in the degree of preferential orientation of the hexagonal carbon layers.

The large difference (more than a factor of ten) between the linear thermal expansion coefficients in two mutually perpendicular directions causes the large internal thermal stresses which appear in pyrographite on cooling[69].

4. Mechanical Properties[4,74,78,80-84]

There are large discrepancies between results obtained by various authors, owing to the lack of a unique method of determining the mechanical properties of pyrographite. Hence, the statements made below should only be accepted as tentative. Like many of its other properties, the strength of pyrographite shows distinct anisotropy. It is highest in the direction parallel to the deposition surface.

(a) The tensile strength increases with temperature (as in the case of polycrystalline graphites). Pappis[80] explains this phenomenon in terms of the increase in plasticity of pyrographite on heating. However, it seems more likely that the increase in strength of pyrographite with temperature is associated with the relief of internal stresses, the closing up of microcracks, and the increase in area of contacting surfaces on heating.

The temperature coefficient of the tensile strength depends on the deposition temperature (Fig. 11), and to a lesser degree on the size of the conical fragments.

A decrease in grain size makes the appearance of internal stresses less likely, and thus raises the strength of these materials.

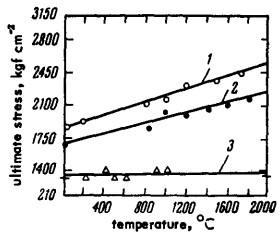


Fig.11. Temperature variation of the tensile and bend strengths of pyrographite:
1) bend strength[80] with load applied parallel to the *c* axis;
2) bend strength with load applied normal to the *c* axis;
3) ultimate tensile stress[85].

One of the main differences between pyrolytic graphite and the normal polycrystalline graphite carbons is the steady increase in strength of the former up to temperatures[83] in excess of 3000°.

(b) The bend strength increases with decreasing size of the conical formations, again because of the decreased probability of crack formation. This parameter also increases slightly with the temperature of the measurement (Fig. 11).

(c) The elongation increases from 0.1% at room temperature to 24% and 59.2% at 2500° and 2750° respectively[74]. At 1650° the elongation of pyrographite is higher than that of any other form of synthetic graphite.

5. Thermal Conductivity[8-9,69,71,73,74,80-82,84,86,87]

It is evident, from the data of Table 3, that the anisotropy coefficient at 300°K can vary from 50 to 100 according to the conditions under which the pyrographite is prepared[87]. In the direction parallel to the deposition surface the thermal conductivity can be as high as 320 kcal m^{-1} h^{-1} deg^{-1}, which is higher than the thermal conductivity of copper, whereas in the perpendicular direction it has a value of the order of 1–3 kcal m^{-1} h^{-1} deg^{-1}, which corresponds to the best high-temperature thermal insulants.

The temperature dependence of the thermal conductivity of various types of pyrographite is shown in Fig. 12. It is determined by phonon–phonon interactions and by the size of the crystallites. The curves go through a maximum at 50–100°K. Below these temperatures $K_\perp$ is proportional to T^α, where α lies between 2.3 and 2.8. These data show that the anisotropy coefficient of the thermal conductivity of pyrographite is also a function of temperature.

TABLE 3. Thermal conductivity of pyrographite.

Specimen	Density, g cm^{-3}	Thermal conductivity, kcal m^{-1} h^{-1} deg^{-1}			Thermal anisotropy $K_\parallel/K_\perp$
		measurement temperature, °K	$K_\perp$	$K_\parallel$	
Raytheon pyrographite (Ref. 87)	2.10	300	2.25	215	95
Raytheon pyrographite (Ref. 87)	2.17	300	2.95	320	110
General Electric pyrographite (Ref. 87)	2.19	300	1.24	57	46

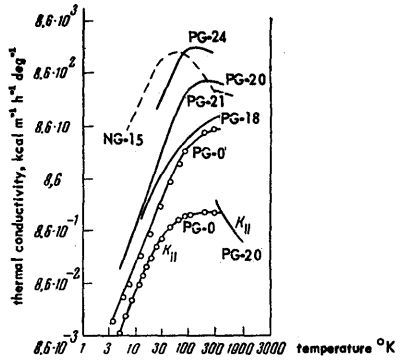


Fig.12. Temperature dependence of the thermal conductivity of various specimens of pyrographite (PG) and natural graphite (NG) at right angles to the *c* axis, after Slack[87]. Values of $K_\parallel$ (parallel to the *c* axis) are given only for two specimens. NG-15, Canadian natural graphite; PG-24, National Carbon pyrographite; PG-21, Royal Aircraft Establishment pyrographite; PG-20, Raytheon pyrographite; PG-18, National Carbon pyrographite; PG-0, General Electric pyrographite.

6. Electrophysical Properties

(a) Electrical resistivity. Fig. 13, based on Klein's results[88], shows the effect of deposition temperature on the electrical resistivity in a direction parallel to the deposition surface (see also Table 4).

The curve of Fig. 13 can be divided into sections corresponding to the following temperature ranges: 1100–1700°, in which the curve slopes gently; 1700–2000°, where the electrical resistance falls sharply (by about a factor of ten); above 2000°, where the curve slopes gently again.

This curve has a characteristic similarity to the behaviour of conventional well graphitised materials. However, the inflections occur at lower temperatures with the latter materials, and the resistance in the direction of the

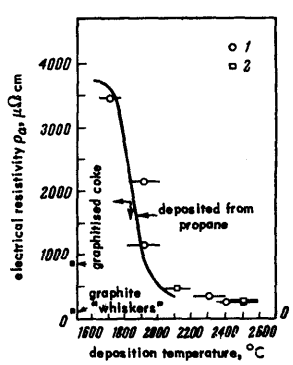


Fig.13. Effect of deposition temperature[88] on the electrical resistivity of pyrographite in the direction of the *a* axis:
1) pyrographite prepared in an induction furnace;
2) pyrographite prepared in a resistance furnace.

TABLE 4. Electrical resistivity at 20° of pyrographite and some graphites.

Materials	Resistivity, Ω mm² m⁻¹		Anisotropy ρ_a/ρ_c
	ρ_a	ρ_c	
Pyrographite[88] prepared at 2500°	3	11000	3670
Graphite single crystals[89,90]	0.4	50	125
Graphite "whiskers"[91]	0.5	—	—
Synthetic graphite	10	—	—

deposition plane is much lower in the case of pyrographite. This is yet another manifestation of the sharp structural anisotropy of pyrographite. However, the electrical resistance in the direction of the *a* axis is about an order of magnitude higher than in a graphite single crystal.

For the reasons already discussed, the resistance at right angles to the deposition surface increases with deposition temperature. This gives rise to a large increase in the anisotropy of the electrical resistivity with increase in deposition temperature. As Klein points out[88], this effect is intimately related to the structural anisotropy of the material (n_{max}/n_{min}, measured by X-ray diffraction as described above).

(b) Magnetic susceptibility. The magnetic susceptibility of pyrographite, like that of other graphitic carbons, is of the diamagnetic type. This is explained by the aromatic structure of the carbon network.

Table 5 gives the diamagnetic susceptibility of pyrographite specimens (after Fishbach[10]), together with susceptibility data for single crystals.

The diamagnetic susceptibility of pyrographite was measured in two mutually perpendicular directions: $\chi_{\parallel}$ and $\chi_{\perp}$ (parallel and perpendicular to the deposition surface, respectively). The measurements were made by the Gouy balance method; the average susceptibility was calculated by the expression $\chi_{av} = \chi_{\perp} + 2\chi_{\parallel}$ CGS deg^{-1}.

It is clear from the data in Table 5 that the anisotropy of the diamagnetic susceptibility of pyrographite increases after heat treatment.

The effect of the heat-treatment temperature on the average magnetic susceptibility of pyrographite prepared at 2100–2300° is shown in Fig. 14. The susceptibility minimum found at 2900° is due to the removal of structural defects at these temperatures. Pyrographite prepared at 1900–2000° shows very small changes in susceptibility with the temperature of heat treatment.

TABLE 5. Diamagnetic susceptibility of pyrographite and of single crystals of natural graphite at 20°, 10^6 CGS g^{-1}.

Materials	χ_{av}	$\chi_{\perp}$	$\chi_{\parallel}$	$\chi_{\perp}/\chi_{\parallel}$
Pyrographite prepared at 2100° (after Fishbach (Ref. 10)	27.3	21.6	2.8	8
Same specimen, heat treated at 2900°	20.0	17.8	1.1	16
Same specimen, heat treated at 3400°	20.7	19.0	0.8	24
Single crystals of natural graphite, data by Poquet *et al.* (Ref. 92)	21.7	21.0	0.3	66
data by Krishnan and Ganguli (Ref. 93)	23.0	22.0	0.5	44

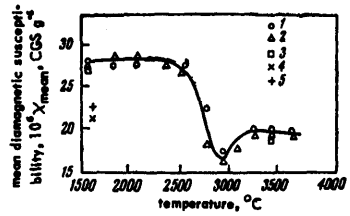


Fig. 14. Variation of the mean diamagnetic susceptibility of pyrographite with temperature of heat treatment (after Fishbach[10]):
1) pyrographite deposited at 2200–2300°;
2) pyrographite deposited at 2100°;
3) pyrographite deposited at 2200°;
4) from Ref. 92;
5) from Ref. 93.

(c) Hall coefficient. The following conclusion can be drawn from the variation of Hall coefficient and degree of graphitisation with deposition temperature[88], shown in Fig. 15.

(1) Pyrographite deposits offer a very wide range of electrophysical properties.

(2) The sign of the Hall coefficient changes twice over the range of deposition temperatures: from minus to plus when deposition occurs at 1500–1600° and from plus to minus at 2100–2200°.

(3) The highest value of the Hall coefficient in the *p*-region occurs at about 1800–1900°, as compared with 2000–2100° for conventional well-graphitised carbons. This same reduction by 200 deg in the critical temperature occurs also, as stated above, in the curve of electrical resistivity against deposition temperature: it is indicative of lower-temperature processes taking part in the formation of intermediate structures in the case of pyrographite.

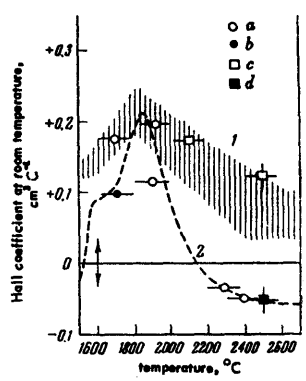


Fig. 15. Effect of deposition temperature on the Hall coefficient of pyrographite[88]:
1) carbon black region;
2) curve for pyrographite;
a) prepared in an induction furnace;
b) the same, after heat treatment;
c) prepared in a resistance furnace;
d) the same, after heat treatment.

TABLE 6. Hall coefficients of some graphitic structures.

Materials	R_H, cm³ C⁻¹
Pyrolytic graphite[88] prepared in a resistance furnace at 2000°	+0.12
Pyrolytic graphite, heat treated[88] at 2600°	−0.05
Single-crystal natural graphite[94]	−0.05
Industrial *p*-type graphite	+0.30
Industrial *n*-type graphite	−0.01

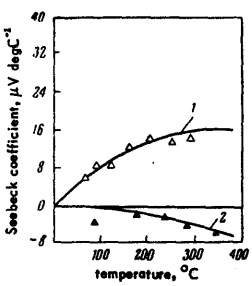


Fig.16. Temperature dependence of the Seebeck coefficient of pyrographite[89]:
1) as prepared;
2) heat treated at 3000°.

This can be explained in terms of the preferential orientation of the hexagonal layers in pyrographite, facilitating the subsequent structural transformations which ultimately determine the electronic properties.

(4) The *p*-region of the Hall curve corresponds to a degree of graphitisation $\gamma \leq 0.6$. In this region we observe the highest development of structural defects which act as "traps" for electrons and thus give rise to positive holes.

(5) Heat treatment which causes γ to increase beyond $\gamma = 0.5$ can also convert pyrographite from the *p* to the *n* conduction type (see also Table 6).

(6) This latter circumstance offers the possibility of realising *p*-*n* junctions in thick layers of pyrographite heat treated at different temperatures. These can be used as high-temperature thermoelements.

Fig. 16 shows the change in Seebeck coefficient with temperature for a *p*-*n* junction in a flat wafer of pyrographite. The *p*-region of graphitised carbons is known[94-99] to conduct by both electrons and holes. The changes in Hall coefficient in this case are due to recombination effects arising from electron–hole interactions in the pyrographite. At the appropriate concentrations of the two types of carrier, and making allowance for the difference in mobility of electrons and holes, conditions for the minimal concentration of uncompensated positive charges (holes) can arise. These correspond to the maximum in the Hall curve.

VI. USES OF PYROGRAPHITE

The high heat resistance, strength, and density of pyrographite, in conjunction with a highly anisotropic thermal conductivity, enable this material to be used in ultra-high-temperature technology as a highly heat-resisting constructional material and for thermal insulation[100-112]. It has been reported[3,6,83,86,101,108-110,113-115] that pyrographite can be used successfully as an erosion-resistant coating for the nozzles of rocket motors, combustion chambers, and nosecones. The properties of pyrographite are said to be superior to those of the best grades of graphite, previously used for these purposes.

Since pyrographite is a practically non-porous material, it has an interesting application as a moderator in nuclear technology. There has been a report[116] of particles of uranium or thorium dicarbide being covered with a 50–100 μm layer of pyrographite and mixed with graphite to produce the heat-evolving elements of a reactor.

The freedom from pores and high corrosion resistance of pyrolytic graphite enable it to be used in the chemical industry as a replacement for scarce metals. Furthermore, vacuum-tight and chemically stable high-temperature materials can be produced by filling the pores of conventional graphitised carbon ware with pyroltyic graphite[19-20].

Graphite tubes, coated with pyrolytic graphite, have proved highly satisfactory as heater elements for electrical resistance furnaces[117].

The unique electrical properties of pyrographite offer a wide scope for applications in electronics (various types of resistor, shunts, etc.)[16-18].

As stated above, the thermoelectric properties of pyrographite enable *p*-*n* junctions to be prepared in the material, and offer the possibility of using pyrographite in high-temperature thermocouples and thermoelements. The recent measurements by Rupprecht *et al.*[118] of the Seebeck coefficient of various pyrographites confirm this prediction.

Thin films of pyrographite show interesting optical properties[83], including that of optical anisotropy. The absorption coefficient for electromagnetic waves is a function of the direction of polarisation, as is the reflectivity. Thus, thin films of pyrographite can be used to polarise infrared radiation[119].

1. C.R.Kinney and E.Del Bel, Ind.Eng.Chem., 46, 548 (1954).
2. A.P.Rudenko, Vestnik Moskov.Univ., Ser.II, No.5, 69 (1960).
3. Materials in Design Eng., 52, 165 (1960).
4. H.E.Martens and L.D.Jaffe, J.Appl.Phys., 31, 1122 (1960).
5. C.A.Klein, Internat.Sci.and Technol., No.8, 60 (1960).
6. Aviation Week, 73, No.4, 28 (1960).
7. A.R.G.Brown, W.Watt, R.W.Powell, and R.P.Tye, Brit.J. Appl.Phys., 7, 73 (1956).
8. A.R.G.Brown and W.Watt, in "Industrial Carbon and Graphite", Society of Chemical Industry, London, 1958, p.86.
9. W.W.Lozier and M.B.Manofsky, "Mechanical Properties of Engineering Ceramics", Interscience, New York, 1961, p.451.
10. D.B.Fishbach, Phys.Rev., 123, 1613 (1961).
11. W.A.Bone and M.F.Coward, J.Chem.Soc., 93, 1197 (1908).
12. W.E.Slater, J.Chem.Soc., 109, 160 (1916).
13. T.S.Wheeler, Fuel, 10, 175 (1931).
14. G.Porter, "Fourth Symposium (International) on Combustion", 1953, p.248.
15. R.J.Diffendorf, J.Chim.phys., 57, 815 (1960).
16. A.C.Pfister, Bell Lab.Record, 26, 401 (1948).

17. R.O.Grisdale, A.C.Pfister, and W.van Roesbroeck, Bell System Tech.J., 30, 271 (1951).
18. G.Bacherez, Z.phys.Chem.(Leipzig), 205, 208 (1955/1956).
19. W.Watt, R.L.Bickerdike, A.R.G.Brown, W.Johnson, and G.Huges, Nuclear Power, 4, No.34, 85 (1959).
20. P.A.Tesner and I.M.Timofeeva, Khim.Prom., No.3, 52 (1962).
21. C.P.Fenimore and J.W.Jones, "Sixth Symposium (International) on Combustion, 1956" (Combustion Institute), Reinhold, New York, 1957, p.242.
22. Ch'ien Shu-an, "Issledovanie Protsessa Obrazovaniya Vtorichnogo Ugleroda na Poverkhnosti Koksa" (Investigation of the Formation of Secondary Carbon at the Surface of Coke), Dissertation, Mendeleev Moscow Institute of Chemical Technology, 1960.
23. I.L.Mar'yasin and P.A.Tesner, Trudy Vses.Nauch.Issled. Inst.Prirodnykh Gazov, No.12 (20), 195 (1961).
24. I.L.Mar'yasin and P.A.Tesner, Dokl.Akad.Nauk SSSR, 140, 1121 (1961).
25. P.A.Tesner and I.S.Rafal'kes, in "Pererabotka i Transport Prirodnykh Gazov" (Treatment and Transport of Natural Gases), Gostoptekhizdat, 1953, p.3.
26. P.A.Tesner and I.S.Rafal'kes, Dokl.Akad.Nauk SSSR, 87, 821 (1952).
27. P.A.Tesner and A.I.Echeistova, in "Pererabotka i Transport Prirodnykh Gazov" (Treatment and Transport of Natural Gases), Gostoptekhizdat, 1953, p.63.
28. P.A.Tesner and A.I.Echeistova, Dokl.Akad.Nauk SSSR, 87, 1029 (1952).
29. P.A.Tesner, Dokl.Akad.Nauk SSSR, 110, 620 (1956).
30. Z.V.Ievleva and P.A.Tesner, Trudy Vses.Nauch.Issled. Inst.Prirodnykh Gazov, No.9, 100 (1957).
31. I.S.Rafal'kes and P.A.Tesner, Trudy Vses.Nauch.Issled. Inst.Prirodnykh Gazov, No.3 (11), 3 (1958).
32. E.Ya.Robinovich and A.V.Rodionov, Trudy.Vses.Nauch. Issled.Inst.Prirodnykh Gazov, No.6 (14) (1959).
33. E.Ya.Robinovich and I.S.Rafal'kes, Trudy Vses.Nauch. Issled.Inst.Prirodnykh Gazov, No.6 (14), 47 (1959).
34. P.A.Tesner, Gazovaya Prom., No.2, 45 (1960).
35. P.A.Tesner, Gazovaya Prom., No.2, 48 (1961).
36. K.Fischer, Brennstoff-Chem., 9, 309 (1928).
37. G.Colligan and F.Galasso, Nature, 190, 4776 (1961).
38. J.S.Conroy, R.S.Slysh, D.B.Murphy, and C.R.Kinney, in "Proceedings of the Third Conference on Carbon", Pergamon, New York, 1959, p.395.
39. C.R.Kinney, R.C.Nunn, and P.D.Walker, Ind.Eng.Chem., 49, 880 (1957).
40. J.D.Frazee and R.C.Anderson, in "Proceedings of the Third Conference on Carbon", Pergamon, New York, 1959, p.405.
41. M.P.E.Berthelot, Ann.Chim.Phys., 9, 451 (1866).
42. F.C.Stehling, J.D.Frazee, and R.C.Anderson, "Sixth Symposium (International) on Combustion, 1956" (Combustion Institute), Reinhold, New York, 1957, p.247.
43. M.N.Plooster and T.B.Reed, J.Chem.Phys., 31, 66 (1959).
44. E.H.Hague and R.V.Wheeler, J.Chem.Soc., 378 (1929).
45. K.Fischer, "Proceedings of the Second International Conference on Bituminous Coals", Vol.2, 1928, p.789.
46. F.P.Rice, W.R.Johnson, and B.L.Evering, J.Amer.Chem. Soc., 54, 3529 (1932).
47. F.P.Rice and M.D.Dooley, J.Amer.Chem.Soc., 56, 214 (1934).
48. L.Belchetz and E.K.Rideal, Trans.Faraday Soc., 30, 170 (1934).
49. G.S.Eltenton, J.Chem.Phys., 15, 455 (1947).
50. R.O.Grisdale, J.Appl.Phys., 24, 1288 (1953).
51. J.E.Zanett and G.Egloff, Ind.Eng.Chem., 9, 350 (1917).
52. B.T.Brooks, Ind.Eng.Chem., 18, 521 (1926).
53. G.Egloff, "Reactions of Pure Hydrocarbons", Reinhold, New York, 1937.
54. D.B.Murphy, H.B.Palmer, and C.R.Kinney, in "Industrial Carbon and Graphite", Society of Chemical Industry, London, 1958, p.77.
55. R.Holdeman and M.Botty, J.Phys.Chem., 63, 4 (1959).
56. N.I.Kobozev, Zhur.Obshch.Khim., 5, 141 (1935).
57. M.D.Tilicheev and V.K.Shchitkova, Neftyanoe Khozyaistvo, No.1, 51 (1937).
58. V.A.Poltorak and V.V.Voevodskii, Dokl.Akad.Nauk SSSR, 91, 589 (1953).
59. G.V.Benevolenskaya and V.P.Kel'tsev, Trudy Vses.Nauch. Issled.Inst.Prirodnykh Gazov, No.3 (11), 116 (1958).
60. P.S.Shantarovich and B.V.Pavlov, Zhur.Fiz.Khim., 34, 960 (1960) [Russ.J.Phys.Chem., 456 (1960)].
61. A.A.Vvedenskii and A.V.Frost, Zhur.Obshch.Khim., 2, 542 (1932).
62. G.Glockler, J.Chem.Phys., 22, 159 (1954).
63. M.C.Chen, C.J.Christensen, and H.Eyring, J.Phys.Chem., 59, 1146 (1955).
64. D.I.Mendeleev, "Osnovy Khimii" (Fundamentals of Chemistry), Vol.1, Goskhimizdat, Moscow–Leningrad, 1947.
65. V.I.Kasatochkin, Dokl.Akad.Nauk SSSR, 86, 759 (1952).
66. O.J.Guentert and C.T.Prewitt, Bull.Amer.Phys.Soc., 5, 187 (1960).
67. O.J.Guentert and S.Cvikevich, Acta Cryst., 13, 12 (1960).
68. A.S.Fialkov, Ya.G.Davidovich, K.V.Kononova, and I.M.Yurkovskii, Dokl.Akad.Nauk SSSR, 153, 390 (1963).
69. L.C.F.Blackman and A.R.Ubbelohde, Proc.Roy.Soc., 266A, 20 (1962).
70. R.H.Bragg and C.M.Packer, Nature, 195, 1080 (1962).
71. V.I.Kasatochkin and A.T.Kaverov, Dokl.Akad.Nauk SSSR, 117, 837 (1958).
72. R.E.Franklin, Proc.Roy.Soc., 209A, 196 (1951).
73. A.R.G.Brown, D.Clark, and J.Eastabrook, J.Less--Common Metals, 1, 94 (1959).
74. H.E.Martens and W.M.Kotlensky, Nature, 186, 960(1960).
75. W.J.Coy, J.Amer.Chem.Soc., 45, 223 (1962).
76. W.Meier, Schweiz.Arch., 26, 29 (1960).
77. A.R.G.Brown, A.R.Hall, and W.Watt, Nature, 172, 1145 (1953).
78. J.Pappis, "Mechanical Properties of Engineering Ceramics", Interscience, New York, 1961, p.429.
79. J.Pappis, "Conference on High Temperature Materials", Cleveland, Ohio, 1961.
80. J.Pappis and S.L.Blum, J.Amer.Ceram.Soc., 44, 592 (1961).
81. S.L.Blum and J.Pappis, Electronic Progr., 4 (6), 17 (1960).
82. Metal Progr., 78, No.5, 68 (1960).
83. A.Gardner, Product Eng., 33, 72 (1962).
84. C.Malstrom, R.Keen, and L.Green, J.Appl.Phys., 22, 593 (1953).
85. R.J.Diffendorf, in "Proceedings of the Fourth Conference on Carbon" (Edited by S.Mrozowski), Pergamon, New York, 1960, p.483.
86. Materials in Design Eng., 52, No.5, 13 (1960).
87. G.A.Slack, Phys.Rev., 127, 694 (1962).
88. C.A.Klein, Rev.Mod.Phys., 34, 56 (1962).
89. W.Primak and L.H.Fuhs, Phys.Rev., 95, 22 (1954).
90. W.Primak, Phys.Rev., 103, 544 (1956).
91. R.Bacon, J.Appl.Phys., 31, 283 (1960).
92. E.Poquet, N.Lumbroso, J.Hoarau, A.Marchand, A.Pacault, and D.E.Soule, J.Chim.phys., 57, 866 (1960).
93. K.S.Krishnan and N.Ganguli, Nature, 139, 155 (1937).
94. D.E.Soule, Phys.Rev., 112, 698 (1958).
95. G.H.Kinchin, Proc.Roy.Soc., 217A, 9 (1953).
96. S.Mrozowski and A.Chaberski, Phys.Rev., 104, 74 (1956).

97. S.Mrozowski, A.Chaberski, E.E.Loebner, and H.T.Pinnick, "Proceedings of the Third Conference on Carbon", Pergamon, New York, 1959, p.211.
98. O.Hauser, Z.phys.Chem.(Leipzig), 210, 151 (1959).
99. C.A.Klein, J.Appl.Phys., 33, 3338 (1962).
100. Electrical Equipment Eng., 6, No.9, 12 (1958).
101. R.G.Higginbotham and M.J.Kemp, Ceram.Age, 71, No.2, 28 (1958).
102. J.Hove, Trans.AIME, 212, No.2, 7 (1958).
103. J.F.Lynch, I.F.Quirk, and W.H.Duckworth, Bull.Amer. Ceram.Soc., 37, 443 (1958).
104. E.R.Stover, J.Metals, 12, 721 (1960).
105. Angew.Chem., 72, No.2, 17 (1960).
106. A.Hilliard, Chem.Process Eng., 41, 416 (1960).
107. W.M.Gaylord, Ind.Eng.Chem., 51, 1161 (1959).
108. J.Judge, Missiles and Rockets, 7, No.19, 21 (1960).
109. Metal.Progr., 75, 108 (1959).
110. M.Jaffe, Aviation Week, 73, No.4, 26 (1960).
111. Ind.Heat, 27, 2200 (1960).
112. Silikattechnik, No.12, 585 (1960).
113. F.Barrata, ARS, 32, 83 (1962).
114. Materials in Design Eng., 58, 139 (1963).
115. W.F.Kaufman, W.H.Armour, and L.Green, Jnr., ARS, 32, 1600 (1962).
116. Steel, 151, No.6, 89 (1962).
117. A.I.Baver, Yu.E.Zusman, and M.A.Novik, USSR P. 155491 (12th March 1962); Byull.Izobr., No.13 (1963).
118. G.Rupprecht, A.Ulavsky, and P.Smakula, Bull.Amer.Phys. Soc., 8, 337 (1963).
119. G.Rupprecht, D.M.Ginsberg, and G.D.Leslie, J.Opt.Soc. Amer., 52, 665 (1962).
120. A.S.Fialkov, A.I.Baver, M.I.Chaikun, B.N.Smirnov, I.M.Yurkovskii, N.M.Sidorov, and S.M.Rabinovich, Zhur. Strukt.Khim., 6, No.1 (1965).

U. D. C. 541.11 : 541.135

THERMODYNAMICS OF MOLTEN SALTS WITH A COMMON ION

A. N. Kirgintsev and E. G. Avvakumov

CONTENTS

1. Introduction 58
2. Distinguishability of the common ion 58
3. Relation between the exchange energy and the properties of the constituents of the solution 63
4. Calculation of exchange energies 65

1. INTRODUCTION

According to Semenchenko's classification[1], ionic salt solutions belong to the group of homoeodynamic solutions. Hence, solutions of ionic salts can be expected to show the general properties of homoeodynamic solutions.

The theory of homoeodynamic solutions relies to a great extent on statistical methods. However, at least for the time being, any kind of statistical description can give no more than a relatively crude picture of real solutions. We believe, therefore, that simple and clearly defined physical models, whose conclusions can be put to simple experimental test, should prove very valuable in this field. The regular solution model is typical of such models.

According to the theory of regular solutions, the potential energy of formation of a solution, ΔE, is given by the expression

$$\Delta E = \omega N_{AB}, \tag{1}$$

where N_{AB} and ω are respectively, the number of bonds between atoms or molecules of different kinds in the case of atomic or molecular solutions and the average potential energy of one such bond (exchange energy). For solutions of ionic salts, these quantities refer to the number of bonds between ions of different kinds and the average potential energy of one bond. If the solution, composed of the salts $A_{n_1}C_{n_2}$ and $B_{n_3}C_{n_4}$, contains n_1N_1 ions of kind A and n_3N_2 ions of kind B, we have

$$N_{AB} = \frac{n_1N_1 \cdot n_2N_2}{n_1N_1 + n_2N_2}. \tag{2}$$

Since the chemical potential of the ith salt component is given by

$$\mu_i = \mu_{i0} + \frac{\partial \Delta E}{\partial N_i} - T\frac{\partial \Delta S}{\partial N_i}, \tag{2a}$$

it can also be expressed, using Eqns. (1) and (2), in the form

$$\mu_i = \mu_{i0} + \omega\beta_i(1 - x_i)^2 - T\frac{\partial \Delta S}{\partial N_i}, \tag{3}$$

where

$$\beta_1 = \frac{n_1}{\left(x_2 + \frac{n_1}{n_2}x_1\right)^2}, \quad \beta_2 = \frac{n_2}{\left(x_1 + \frac{n_2}{n_1}x_2\right)^2}, \quad x_i = \frac{N_i}{N_1 + N_2}; \tag{4}$$

and μ_{i0} denotes the chemical potential of the ith component in its standard state (taken to be the pure compound); ΔS is the entropy of mixing. In what follows, formulae relating to the first and to the second component of a solution or of a system will be written in that order.

The present article discusses the application of regular solution theory to solutions of ionic salts having a common ion, and considers the relation between the exchange energy ω and the properties of the individual constituents. Considerable use is made of published data as well as of values calculated by the writers.

2. DISTINGUISHABILITY OF THE COMMON ION

The earliest theories of ionic solutions[2,3,4], and some of the later ones[5,6], determine the potential energy of a solution in terms of the ionic radii and the composition. The entropy of mixing is usually assumed equal to the normal entropy of mixing of ideal solutions. This approximation can be too crude when ions of different valencies are involved, since the problem of the entropy of mixing is not considered in those papers.

From the thermodynamic point of view, the formation of an ideal solution presents three independent requirements:

1. The change in potential energy resulting from formation of the solution must be zero.